

Falcarindiol alleviates airway inflammation and oxidative stress in asthma through Nrf2 pathway activation

Received: 23 July 2025

Accepted: 28 January 2026

Published online: 21 February 2026

Cite this article as: Jiang X., Lai S., Lin Z. *et al.* Falcarindiol alleviates airway inflammation and oxidative stress in asthma through Nrf2 pathway activation. *Sci Rep* (2026). <https://doi.org/10.1038/s41598-026-37962-5>

Xiuhua Jiang, Shengxiu Lai, Zhen Lin, Fuhuang Lai & Huifang Wu

We are providing an unedited version of this manuscript to give early access to its findings. Before final publication, the manuscript will undergo further editing. Please note there may be errors present which affect the content, and all legal disclaimers apply.

If this paper is publishing under a Transparent Peer Review model then Peer Review reports will publish with the final article.

Falcarindiol alleviates airway inflammation and oxidative stress in asthma through Nrf2 pathway activation

Xiuhua Jiang^{1*}, Shengxiu Lai^{2*}, Zhen Lin¹, Fuhuang Lai¹, Huifang Wu^{1#}

¹Department of pediatrics, Longyan First Hospital, 364000, China

²Department of pediatrics, Longyan Hospital of Traditional Chinese Medicine, 364000, China

*Equal Contributors

#Corresponding author: No. 1, Lianzhuang South Road, Caoxi Street, Xinluo District,

Longyan City, 364000, Fujian Province, China. Email□
wuhuifang23@163.com

Running title□Falcarindiol alleviates asthma

ARTICLE IN PRESS

Abstract**Background**

Oxidative stress and Th2-type immune responses play pivotal roles in asthma pathogenesis. Falcarindiol (FAD), a natural polyacetylene compound, exhibits promising anti-inflammatory and antioxidant properties, yet its therapeutic mechanism and efficacy in asthma treatment remain to be explored.

Methods

An ovalbumin (OVA)-induced murine asthma model and IL-13-stimulated human bronchial epithelial cells (BEAS-2B) were employed to investigate FAD's therapeutic mechanisms. Airway inflammation, oxidative stress markers, and Nrf2 pathway activation were comprehensively evaluated through hematoxylin and eosin (H&E) staining, ELISA, flow cytometry, and Western blotting. To establish mechanistic causality, the Nrf2 inhibitor ML385 and targeted shRNA knockdown approaches were used to validate the essential role of Nrf2 activation in mediating FAD's protective effects.

Results

In OVA-induced asthmatic mice, FAD (100 or 200 mg/kg) produced dose-dependent therapeutic benefits, significantly reducing inflammatory scores, decreasing airway wall and smooth muscle thickness, substantially lowering serum IgE levels, and diminishing eosinophil infiltration in bronchoalveolar lavage fluid (BALF). Additionally, FAD effectively ameliorated oxidative stress, while simultaneously suppressing pro-inflammatory cytokine release. In IL-13-stimulated BEAS-2B cells, FAD dose-dependently protected against apoptosis and restored proliferation capacity while robustly

activating the Nrf2/HO-1/NQO1 pathway. Mechanistic validation studies revealed that both ML385-mediated Nrf2 inhibition and Nrf2 shRNA knockdown largely abrogated FAD's protective effects.

Conclusion

FAD exerts anti-asthmatic effects through Nrf2 pathway activation, effectively mitigating airway inflammation, oxidative stress, and epithelial injury, establishing it as a promising therapeutic candidate for asthma.

Keywords: Falcarindiol; asthma; Nrf2 pathway; airway inflammation; oxidative stress; airway remodeling

Introduction

Asthma is a heterogeneous chronic respiratory disorder characterized by complex pathophysiological mechanisms. Its pathogenesis is closely linked to persistent bronchial inflammation, which involves the activation and recruitment of multiple inflammatory cells and their associated mediators^[1]. According to World Health Organization (WHO) data, approximately 339 million people worldwide suffer from asthma, with the majority of patients developing symptoms during childhood, particularly in early school years^[2]. Over the past decades, the global prevalence of asthma has increased markedly, posing a significant public health challenge worldwide^[3]. The primary clinical manifestations of childhood asthma encompass recurrent wheezing, dyspnea, chest tightness, and cough. Poor disease control may result in persistent airway dysfunction and long-term respiratory complications. Current therapeutic agents for asthma include glucocorticoids, theophylline derivatives, β_2 -agonists, anticholinergics, and lipoxygenase inhibitors, though these medications are often associated with significant adverse effects^[4]. Therefore, comprehensive

investigation of asthmatic pathogenesis and the identification of novel therapeutic targets are critical for improving treatment efficacy and patient outcomes.

Chronic airway inflammation drives hyperresponsiveness in asthma, manifesting as reversible expiratory airflow obstruction. Key pathological features include eosinophilic infiltration, mucus hypersecretion, airway remodeling, and bronchoconstriction^[5]. Th2-type cytokines orchestrate these inflammatory processes^[6]. IL-13 drives epithelial-to-mucus cell transdifferentiation, promoting goblet cell hyperplasia and airway hyperresponsiveness. IL-4 facilitates IgE class switching and synergizes with IL-13 to produce high-affinity IgE antibodies. Upon allergen exposure, IgE cross-links FcεRI receptors on mast cells and basophils, triggering degranulation and release of bronchoconstrictive mediators including histamine and proteases^[7]. IL-5 regulates eosinophil biology by promoting their proliferation, survival, and airway recruitment. These recruited eosinophils release inflammatory mediators that perpetuate bronchoconstriction^[8-10]. Nuclear factor erythroid 2-related factor 2 (NRF2), also known as nuclear factor E2-related factor 2, is a master transcription factor that coordinates the basal and oxidative stress-induced activation of a vast array of cytoprotective genes including antioxidant enzymes, detoxification proteins, and anti-inflammatory mediators^[11]. NRF2 critically regulates multiple asthmatic pathological processes^[11-13], establishing NRF2 pathway modulation as an attractive therapeutic target.

Traditional Chinese medicine (TCM) has gained significant recognition in asthma therapeutics, with clinical evidence demonstrating that TCM formulations including Maimendong Tang

and Dingchuan Tang provide substantial therapeutic benefits for asthmatic patients worldwide^[14]. Falcarindiol (FAD), a bioactive polyacetylene compound isolated from Apiaceae vegetables, exhibits multifaceted pharmacological properties encompassing anti-tumor, neuroprotective, and anti-inflammatory activities^[15-18]. Mechanistically, FAD selectively activates nuclear factor erythroid 2-related factor 2/antioxidant response element (Nrf2/ARE) signaling through S-alkylation of Kelch-like ECH-associated protein 1 (Keap1) cysteine 151, leading to Nrf2 nuclear translocation and antioxidant gene expression^[19]. Given that Nrf2 pathway dysfunction underlies oxidative stress and chronic inflammation in asthma pathogenesis^[11-13], we hypothesized that FAD could ameliorate asthmatic inflammation through Nrf2-mediated mechanisms.

This study aimed to investigate the therapeutic potential of FAD in asthma treatment and elucidate its underlying molecular mechanisms. Using both *in vivo* ovalbumin-induced murine asthma models and *in vitro* interleukin-13-stimulated human bronchial epithelial cells, we systematically evaluated FAD's anti-inflammatory and antioxidant effects. Mechanistic validation was performed through Nrf2 inhibition and knockdown experiments to establish causality between FAD's therapeutic benefits and Nrf2 pathway activation. Our findings demonstrate that FAD significantly ameliorates airway inflammation, reduces oxidative stress, and restores epithelial cell function through Nrf2-dependent mechanisms. These results establish FAD as a promising natural therapeutic candidate for asthma management and provide mechanistic insights supporting the development of Nrf2-targeted anti-asthmatic therapies.

Methods

Establishment of Asthma Mouse Model and FAD Treatment

The animal experiments were approved by the Animal Care and Use Committee at Longyan First Hospital and conducted in strict accordance with institutional and national guidelines for laboratory animal care. Male BALB/c mice aged 6-7 weeks (18-20 g) were procured from Beijing SPF Laboratory Animal Co., Ltd., and maintained in a specific pathogen-free facility under controlled environmental conditions including temperature (22 ± 2 °C), humidity ($50 \pm 10\%$), and a standard 12-hour light/dark cycle with ad libitum access to standard laboratory chow and water. Following a one-week acclimatization period, mice were randomly allocated into experimental groups using a computer-generated randomization sequence.

The dose-intervention experiment comprised five groups (n=6 per group): Sham control, OVA-induced asthma model, OVA + FAD (100 mg/kg), OVA + FAD (200 mg/kg), and OVA + dexamethasone (DEX, 1 mg/kg) as a positive control. Asthma induction was initiated on day 0 with intraperitoneal immunization using 100 μ L of OVA allergen solution (10 μ g) containing aluminum hydroxide adjuvant (1 mg), with the sham control group receiving an equal amount of normal saline^[13]. The sensitization phase was followed by an airway challenge period from days 7-14, during which mice were exposed to aerosolized 1% OVA solution (0.1 g OVA dissolved in 10 mL PBS) for 60 minutes daily using an ultrasonic nebulizer to establish chronic airway inflammation. Therapeutic interventions were administered concurrently with the challenge phase, with FAD (100 or 200 mg/kg ^[20]) dissolved in 0.5% carboxymethylcellulose (CMC)

solution or DEX (1 mg/kg) delivered via oral gavage daily from day 7. The model group received the same volume of solvent (vehicle) via oral administration following the same dosing schedule as the FAD treatment groups, while the sham control group received equivalent volumes of PBS vehicle.

The mechanistic intervention experiment employed four groups (n=6 per group) to validate Nrf2-dependent mechanisms: Sham + lentiviral negative control shRNA, OVA + lentiviral negative control shRNA, OVA + FAD (200 mg/kg) + lentiviral negative control shRNA, and OVA + FAD (200 mg/kg) + lentiviral Nrf2-targeting shRNA. The asthma induction protocol remained identical to the dose-intervention study. To achieve targeted Nrf2 knockdown, lentiviral particles (5×10^7 infectious units in 50 μ L) carrying either scrambled negative control or Nrf2-specific shRNA sequences were delivered via intratracheal lung injection seven days prior to the nebulization challenge period to ensure adequate gene silencing. Mice were anesthetized with isoflurane, and lentiviral particles were administered through direct visualization of the trachea using a laryngoscope, followed by gentle ventilation to ensure uniform pulmonary distribution. FAD treatment (200 mg/kg) dissolved in 0.5% CMC solution was administered daily via oral gavage throughout the challenge phase in designated groups, with control groups receiving equivalent volumes of 0.5% CMC vehicle.

Sample collection and processing were performed 24 hours following the final nebulization exposure. Mice were humanely euthanized via cervical dislocation under isoflurane anesthesia. Bronchoalveolar lavage was performed through tracheotomy using three sequential 0.5 mL aliquots of ice-cold PBS, with gentle aspiration to recover approximately 1.2-1.4 mL of bronchoalveolar lavage fluid (BALF) per animal. The recovered BALF was

immediately centrifuged at 1000 rpm for 10 minutes at 4°C to separate cellular and acellular components. Supernatants were aliquoted and stored at -80°C for subsequent cytokine profiling and oxidative stress marker analysis, while cell pellets were resuspended in PBS for total and differential cell counting using standard hematological techniques. Blood samples were obtained via cardiac puncture and allowed to clot at room temperature before centrifugation to obtain serum, which was stored at -80°C for enzyme-linked immunosorbent assay (ELISA) analysis. Lung tissues were processed using a standardized protocol: the left lung lobe was fixed in 4% paraformaldehyde for 24 hours for histopathological examination, terminal deoxynucleotidyl transferase dUTP nick end labeling (TUNEL) assay, and Ki67 immunofluorescence staining, while the right lung lobe was immediately flash-frozen in liquid nitrogen and stored at -80°C for protein extraction and Western blot analysis.

Assessment of Airway Hyperresponsiveness Using Semi-Quantitative Visual Scoring

Airway hyperresponsiveness (AHR) was evaluated using a semi-quantitative visual scoring method following methacholine challenge. This cost-effective method has been validated in previous studies as a reliable indicator of respiratory distress and bronchial reactivity. Mice were administered a standardized dose of methacholine (25 mg/mL) via nebulization for 30 seconds, and respiratory patterns were continuously observed for 5 minutes post-challenge. Respiratory distress was scored using a validated 0-4 scale: 0 = normal breathing pattern with no observable distress; 1 = slight labored breathing with minimal chest wall retractions; 2 = moderate respiratory distress with visible increased respiratory effort; 3 =

severe labored breathing with pronounced chest wall retractions and reduced activity; 4 = gasping respirations with severe distress and minimal movement. Two independent observers blinded to treatment groups performed the scoring, and the average scores were recorded for analysis.

Hematoxylin-Eosin (H&E) Staining

Following extraction, lung tissues were fixed in 4% paraformaldehyde (Servicebio, Wuhan) for 24 hours, rinsed with phosphate-buffered saline (PBS, Solarbio, Beijing), and processed through standard histological procedures including dehydration in graded ethanol series (70-100%), xylene clearing, and paraffin embedding. Tissue sections (4 μm thickness) were cut using a microtome (Leica, Germany), mounted on glass slides, and subjected to hematoxylin-eosin (H&E) staining (Solarbio, Beijing) following routine deparaffinization. The staining protocol comprised nuclear staining with hematoxylin (5-10 minutes), tap water rinsing for bluing, acid alcohol differentiation (1%), thorough water rinsing, and eosin counterstaining (1-3 minutes), followed by dehydration through graded ethanol (75-100%), xylene clearing, and neutral resin mounting. After air-drying, lung tissue pathological changes were evaluated under optical microscopy (BX53, Olympus, Japan) for assessment of inflammatory infiltration, airway wall thickness, and structural alterations. H&E-stained lung sections were blindly evaluated for inflammatory cell infiltration using a standardized 5-point scoring system: 0, no infiltrating cells; 1, a few scattered cells; 2, a single-layer ring of inflammatory cells; 3, a circumferential ring two to four cells in depth; and 4, a ring more than four cells in depth.

Periodic Acid-Schiff (PAS) Staining

Following fixation in 4% paraformaldehyde for 24 hours, lung tissues were processed through routine histological procedures including PBS washing, graded ethanol dehydration (70-100%), xylene clearing, and paraffin embedding. Sections (4 μm) were cut using a Leica microtome and mounted on glass slides. After deparaffinization, slides were subjected to PAS staining using a commercial kit (Sigma-Aldrich, USA) according to manufacturer's instructions. The protocol included oxidation with 0.5% periodic acid solution (5 minutes), thorough rinsing with distilled water, followed by Schiff reagent treatment (15 minutes), and hematoxylin counterstaining (Solarbio, Beijing) for 3 minutes. After washing, sections were dehydrated through graded ethanol series (75-100%), cleared in xylene, and mounted with neutral resin. Stained sections were examined under an Olympus BX53 microscope (Japan) to evaluate mucus production and goblet cell hyperplasia. To quantify mucus production, PAS-stained sections were randomized, examined blindly, and scored on a 0-4 scale: 0, no goblet cells; 1, <25% goblet cells; 2, 25-50% goblet cells; 3, 50-75% goblet cells; and 4, >75% goblet cells. Inflammatory cell infiltration and goblet cell abundance were evaluated in at least three randomly selected fields per lung section.

Terminal deoxynucleotidyl transferase dUTP nick end labeling (TUNEL)

TUNEL staining was performed using a fluorescent apoptosis detection kit (TUNEL Apoptosis Detection Kit, Servicebio, Wuhan, China) to assess apoptotic cell death in lung tissues. Deparaffinized and rehydrated paraffin sections were treated with proteinase K (20 $\mu\text{g}/\text{mL}$) for 20 minutes at room temperature to enhance membrane permeability, followed by PBS washing. Sections were then

incubated with terminal deoxynucleotidyl transferase (TdT) reaction mixture at 37°C for 1 hour in darkness according to manufacturer's instructions, washed three times with PBS (5 minutes each), and processed for fluorescent detection. After counterstaining nuclei with DAPI, sections were mounted with anti-fade mounting medium and examined under fluorescence microscopy (Eclipse Ni-U, Nikon, Japan). TUNEL-positive apoptotic nuclei displayed green fluorescence, while DAPI-stained nuclei appeared blue, allowing quantitative assessment of apoptotic cells within lung tissue architecture. The negative and positive control staining images were shown in Figure S1A.

Ki67 Immunofluorescence

Ki67 immunofluorescence staining was performed on deparaffinized and rehydrated lung tissue sections to assess cellular proliferation. Antigen retrieval was accomplished by microwave heating in 10 mmol/L EDTA buffer (pH 9.0, Beyotime, Shanghai, China), followed by cooling and PBS rinsing. Sections were blocked with 3% bovine serum albumin (BSA, Solarbio, Beijing, China) for 30 minutes at room temperature to prevent nonspecific binding. Primary antibody incubation was performed using anti-Ki67 antibody (Abcam, ab15580, 1:500 dilution, Cambridge, USA) overnight at 4°C, followed by three PBS washes (5 minutes each) and incubation with fluorescein-conjugated goat anti-rabbit secondary antibody (Abcam) for 1 hour at 37°C. After final PBS washing, nuclei were counterstained with DAPI and sections were mounted with anti-fade mounting medium. Ki67-positive proliferating cells were visualized under fluorescence microscopy (Eclipse Ni-U, Nikon, Japan), with Ki67-positive nuclei displaying green fluorescence and DAPI-stained nuclei appearing blue. The negative IgG isotype control and positive

Ki67 staining images were shown in Figure S1B.

Enzyme-Linked Immunosorbent Assay (ELISA)

ELISA was performed to quantify inflammatory cytokines and immune markers in bronchoalveolar lavage fluid (BALF), serum, and cell culture supernatants using commercial ELISA kits for IgE, IL-1 β , IL-18, IL-4, IL-5 and TNF- α (Elabscience, Beijing, China). Following manufacturer's protocols, samples and standards were added to 96-well microplates and incubated with horseradish peroxidase (HRP)-conjugated detection antibodies at 37°C for 60 minutes. After washing, substrate solutions A and B were added and incubated at 37°C for 15 minutes in darkness, followed by reaction termination with 50 μ L stop solution per well. Optical density at 450 nm was measured using a microplate reader, and analyte concentrations were determined from standard curves.

Biochemical Analysis of Oxidative Stress

Biochemical analysis of oxidative stress markers was conducted to evaluate the antioxidant capacity and lipid peroxidation levels in lung tissue homogenates and cell culture lysates. Commercial assay kits for superoxide dismutase (SOD), glutathione (GSH), catalase (CAT), and malondialdehyde (MDA) were obtained from Elabscience (Beijing, China) and performed according to manufacturer's instructions. SOD activity was measured based on the inhibition of superoxide anion-induced nitrite formation, GSH content was determined using the 5,5'-dithiobis-(2-nitrobenzoic acid) method, CAT activity was assessed by monitoring hydrogen peroxide decomposition, and MDA levels were quantified through thiobarbituric acid reactive substances assay. All samples were processed in duplicate, and absorbance readings were obtained

using a microplate reader at appropriate wavelengths specific to each assay. Results were normalized to protein content and expressed as units per milligram of protein or micromoles per milligram of protein for enzymatic activities and metabolite concentrations, respectively.

Immune Cell Infiltration analysis in Lung Tissue Using a Hematology Analyzer

Analysis of immune cell infiltration in lung tissue was performed to evaluate FAD's effects on inflammatory cell recruitment in the OVA-induced asthma model. Following bronchoalveolar lavage, lung tissues were minced and enzymatically digested using type I collagenase (1 mg/mL) and DNase I (30 µg/mL, Sigma-Aldrich, USA) with agitation at 37°C for 30-45 minutes, then filtered through a 200-mesh sieve to generate single-cell suspensions and terminated with RPMI-1640 medium. After centrifugation (1000 rpm, 5 minutes), cell pellets were treated with red blood cell lysis buffer (Solarbio, Beijing, China) for 5 minutes, washed with PBS, and resuspended for analysis using an automated hematology analyzer (Mindray BC-5000Vet, Mindray, Shenzhen, China). Total leukocyte counts and immune cell subtype proportions, including eosinophils and lymphocytes, were quantified to assess FAD's impact on pulmonary inflammatory cell infiltration.

Western Blot

Total protein extraction from lung tissues and cell samples was performed using RIPA lysis buffer, with protein concentrations determined by bicinchoninic acid (BCA) assay. Equal protein amounts (30-50 µg) were separated by 10% sodium dodecyl sulfate-polyacrylamide gel electrophoresis (SDS-PAGE) and transferred

onto polyvinylidene fluoride (PVDF) membranes. Following blocking with 5% non-fat milk for 1 hour at room temperature, membranes were incubated overnight at 4°C with primary antibodies including anti-NRF2 (1:1000, ab62352), anti-Lamin B1 (1:1000, ab16048), anti-heme oxygenase-1 (HO-1, 1:1000, ab305290), anti-NAD(P)H quinone dehydrogenase 1 (NQO1, 1:1000, ab80588), and anti- β -actin (1:2000, ab8226, all from Abcam, Cambridge, UK). After washing, membranes were incubated with horseradish peroxidase (HRP)-conjugated secondary antibodies for 1 hour at room temperature. Protein signals were visualized using enhanced chemiluminescence (ECL) detection and captured with a Tanon 5200 imaging system (Tanon, Shanghai, China), with β -actin serving as the loading control for band intensity normalization. [Quantification of immunoblots was analyzed using ImageJ 1.53k \(https://imagej.nih.gov/ij/\)](https://imagej.nih.gov/ij/).

Cell Culture and Treatment

The human bronchial epithelial cell line BEAS-2B (iCell-h023, iCell Bioscience, Shanghai, China) was maintained in RPMI-1640 medium (Hyclone, USA) supplemented with 10% fetal bovine serum (FBS, Gibco, USA) and 1% penicillin-streptomycin (Gibco, USA) in a humidified incubator at 37°C with 5% CO₂. Cells were randomly assigned to four experimental groups for mechanistic studies. The control group received no treatment, while the IL-13 group was stimulated with human recombinant interleukin-13 (10 ng/mL, Stemcell, USA) for 24 hours to establish an asthma-like inflammatory cellular model. The IL-13 + FAD group received falcariindiol (FAD, HY-N0364, MCE, Shanghai, China) treatment (5-20 μ M) following IL-13 stimulation to evaluate therapeutic effects, and the IL-13 + FAD + ML385 group was co-treated with FAD and the NRF2 pathway inhibitor ML385 (SML1833, 10 μ M, Sigma-Aldrich, USA)

after IL-13 stimulation to validate NRF2-dependent mechanisms. All treatments were performed for 24 hours, followed by cell viability assessment, apoptosis analysis, and protein expression evaluation.

CCK-8 Cell Viability Assay

BEAS-2B cells were seeded into 96-well plates at a density of 5×10^3 cells per well and allowed to adhere overnight before experimental treatments. After completion of treatments, 10 μ L of CCK-8 reagent (CK04, Dojindo, Japan) was added to each well and incubated for 2 hours at 37°C under 5% CO₂. Cell viability was determined by measuring absorbance at 450 nm using a microplate reader, with results expressed as percentage viability relative to untreated control cells.

EdU Incorporation Assay

Cell proliferation was assessed using the Click-iT™ Plus EdU Cell Proliferation Kit for Imaging with Alexa Fluor™ 594 dye (C10639, Invitrogen™, Thermo Fisher Scientific, USA). Following experimental treatments, BEAS-2B cells were incubated with 10 μ M 5-ethynyl-2'-deoxyuridine (EdU) for 2 hours at 37°C under 5% CO₂ to label DNA synthesis during S-phase. Cells were then fixed with 4% paraformaldehyde for 15 minutes, permeabilized with 0.1% Triton X-100 for 10 minutes, and processed according to manufacturer's protocol. The Click-iT™ reaction was performed using the provided copper catalyst solution and Alexa Fluor™ 594 azide for 30 minutes at room temperature in darkness. Nuclei were counterstained with DAPI, and cells were examined under fluorescence microscopy (Eclipse Ni-U, Nikon, Japan). Proliferating cells displayed red fluorescence (EdU-positive), while all nuclei appeared blue (DAPI), allowing quantification of proliferation rates as the percentage of

EdU-positive cells relative to total cell count.

Flow Cytometry of Cell Apoptosis

Apoptosis analysis was performed using flow cytometry with the Annexin V-FITC Apoptosis Detection Kit. BEAS-2B cells (1×10^6 cells) were collected, washed twice with ice-cold PBS, and resuspended in 300 μ L of $1 \times$ Annexin V binding buffer (BD Biosciences, USA). Cells were incubated with 5 μ L Annexin V-FITC (1 μ g/mL) for 15 minutes at room temperature in darkness, followed by addition of 5 μ L propidium iodide (PI, 50 μ g/mL, BD Biosciences, catalog #556547). Early and late-stage apoptosis was quantified using a flow cytometer (BD FACSCanto II, BD Biosciences, USA), and data analysis was performed using FlowJo software (Tree Star, USA). Results were expressed as percentage of apoptotic cells in each treatment group.

Statistical Analysis

Statistical analysis was performed using GraphPad Prism version GraphPad Prism 9.5.1 software (<https://www.graphpad.com/>, GraphPad Software, San Diego, CA, USA), with data expressed as mean \pm standard deviation (SD) from at least three independent experiments. Normality of data distribution was assessed using the Shapiro-Wilk test. Comparisons between two groups were conducted using unpaired Student's t-test, while multiple group comparisons were evaluated by one-way analysis of variance (ANOVA) followed by Tukey's honest significant difference (HSD) post hoc test for pairwise comparisons. Statistical significance was defined as $P < 0.05$.

Results

FAD Alleviates Airway Inflammation and Suppresses Immune

Cell Infiltration in Asthmatic Mice

To evaluate the therapeutic efficacy of falcarindiol (FAD) in allergic asthma, we employed an ovalbumin (OVA)-induced murine asthma model to assess its effects on airway inflammation, immune responses, and cellular infiltration. Histopathological analysis revealed that FAD treatment dose-dependently reduced inflammatory cell infiltration, airway wall thickening, and smooth muscle hypertrophy, with morphometric quantification confirming significant improvements in inflammation scores and structural remodeling parameters (Wall/Pbm and Wasm/Pbm ratios) (Fig. 1A). PAS staining demonstrated markedly increased mucus-secreting goblet cells and mucus hypersecretion in the bronchial epithelium of OVA-challenged mice, whereas FAD treatment significantly attenuated goblet cell hyperplasia and mucus production in a dose-dependent manner (Fig. 1B). Concurrently, FAD treatment effectively suppressed allergic immune responses by significantly reducing both total and OVA-specific serum IgE levels (Fig. 1C). FAD treatment significantly reduced the elevated serum levels of Th2 cytokines IL-4 and IL-5 in the asthma model group (Fig. 1C). The analysis of BALF demonstrated marked reductions in CD45⁺ leukocyte accumulation and eosinophil infiltration compared to OVA-challenged group (Fig. 1D). Furthermore, the OVA-model group exhibited significantly elevated respiratory distress scores following methacholine challenge, while FAD treatment dose-dependently reduced these scores, indicating improved airway hyperresponsiveness and bronchial reactivity (Fig. 1E). Notably, the therapeutic efficacy of FAD at 200 mg/kg was comparable to that of dexamethasone (DEX), a standard anti-inflammatory corticosteroid, across all measured parameters, suggesting FAD's potential as an effective alternative therapeutic intervention (Fig 1A-1E). These

findings collectively establish that FAD ameliorates cardinal pathophysiological features of experimental asthma through coordinated suppression of airway inflammation, structural remodeling, and immune cell recruitment.

FAD Attenuates Oxidative Stress and Inflammatory Responses Concurrent with Nrf2 Pathway Activation

To elucidate the mechanistic basis of FAD's therapeutic effects, we comprehensively analyzed oxidative stress markers, inflammatory mediators, and Nrf2 pathway activation in asthmatic mice. OVA challenge induced substantial oxidative damage, evidenced by significantly elevated malondialdehyde (MDA) levels and decreased activities of key antioxidant enzymes including superoxide dismutase (SOD), catalase (CAT), and glutathione peroxidase (GSH-Px) in lung tissues compared to sham controls. FAD treatment dose-dependently counteracted these oxidative alterations, reducing MDA accumulation while restoring antioxidant enzyme activities (Fig. 2A-D). In parallel, analysis of bronchoalveolar lavage fluid revealed that while OVA challenge markedly elevated pro-inflammatory cytokines IL-1 β , IL-18, and TNF- α , FAD intervention significantly attenuated these responses in a dose-dependent manner (Fig. 2E-G). This anti-inflammatory efficacy extended systemically, as demonstrated by comparable reductions in serum cytokine concentrations (Fig. 2H-J). Mechanistically, Western blot analysis revealed that OVA-induced suppression of nuclear Nrf2 and downstream targets HO-1 and NQO1 was markedly reversed by FAD treatment (Fig. 2K). These integrated findings demonstrate that FAD's therapeutic benefits occur concurrent with Nrf2 pathway activation, suggesting coordinated enhancement of antioxidant defenses and suppression of inflammatory cascades that collectively ameliorate asthmatic

pathophysiology.

FAD Suppresses Bronchial Epithelial Cell Apoptosis and Restores Proliferation in Asthmatic Mice

To evaluate FAD's regulatory effects on pulmonary epithelial cell fate, we performed TUNEL staining and Ki67 immunofluorescence analysis on lung tissue sections. TUNEL staining revealed substantially increased apoptotic cell populations (TUNEL⁺) in OVA-challenged lungs compared to sham controls, while FAD treatment at all tested doses markedly reduced apoptotic cell counts, demonstrating significant cytoprotective effects comparable to dexamethasone (DEX) (Fig. 3A). Meanwhile, Ki67 immunofluorescence analysis showed that OVA challenge severely suppressed proliferative activity within lung epithelium, whereas FAD intervention dose-dependently restored both Ki67⁺ cell numbers and fluorescence intensity (Fig. 3B). These complementary findings suggest that FAD exerts dual regulatory effects on lung epithelial homeostasis by simultaneously inhibiting pathological apoptosis and promoting regenerative proliferation.

FAD Attenuates IL-13-Induced Apoptosis and Proliferation Suppression in BEAS-2B Cells

To validate FAD's protective effects at the cellular level, we employed IL-13-stimulated human bronchial epithelial BEAS-2B cells as an *in vitro* model of asthmatic epithelial dysfunction. Initial cytotoxicity screening using CCK-8 assay demonstrated that FAD exhibited no adverse effects on cell viability at concentrations up to 20 μ M, with only minimal reduction observed at 50 μ M, establishing 5, 10, and 20 μ M as optimal therapeutic concentrations for subsequent investigations (Fig. 4A). Under IL-13-induced

inflammatory stress, FAD dose-dependently counteracted the suppression of cell viability, effectively reversing IL-13-mediated cytotoxic effects (Fig. 4B). This cytoprotective response was accompanied by restoration of proliferative capacity, as evidenced by EdU immunofluorescence analysis showing that while IL-13 significantly reduced EdU⁺ proliferating cells, FAD treatment progressively restored proliferative cell populations in a concentration-dependent manner (Fig. 4C). Additionally, flow cytometric analysis revealed that FAD effectively mitigated IL-13-induced apoptosis, with dose-dependent reductions in apoptotic cell percentages (Fig. 4D). These cellular findings corroborate the *in vivo* observations, demonstrating that FAD comprehensively protects bronchial epithelial cells against inflammatory injury through coordinated enhancement of viability, proliferation, and survival mechanisms.

FAD Reduces IL-13-Induced Oxidative Stress and Inflammation in BEAS-2B Cells Concurrent with Nrf2 Pathway Activation

To investigate the molecular mechanisms underlying FAD's cytoprotective effects, we examined oxidative stress responses and inflammatory mediator production in IL-13-stimulated BEAS-2B cells. IL-13 challenge induced pronounced oxidative imbalance, characterized by significantly decreased activities of antioxidant enzymes (SOD, CAT, and GSH-Px) and concomitant elevation of lipid peroxidation marker MDA. FAD treatment dose-dependently counteracted these oxidative alterations, restoring antioxidant enzyme activities while reducing MDA accumulation (Fig. 5A-D). In parallel with oxidative stress amelioration, FAD effectively suppressed inflammatory responses, as demonstrated by ELISA

analysis showing that while IL-13 stimulation markedly elevated pro-inflammatory cytokine levels (IL-1 β , IL-18, and TNF- α) in cell culture supernatants, FAD intervention dose-dependently attenuated these inflammatory mediators (Fig. 5E-G). Mechanistically, Western blot analysis revealed that IL-13-induced suppression of nuclear Nrf2 translocation and downregulation of downstream antioxidant proteins HO-1 and NQO1 were markedly reversed by FAD treatment at 20 μ M (Fig. 5H). These in vitro findings corroborate the in vivo observations, demonstrating that FAD's protective effects against oxidative stress and inflammation occur concurrent with Nrf2 pathway activation, suggesting this signaling cascade as a key mediator of FAD's therapeutic benefits.

Nrf2 Pathway is Indispensable for FAD's Protective Effects Against IL-13-Induced BEAS-2B Cell Injury

To establish the mechanistic dependency of FAD's protective effects on Nrf2 signaling, we employed the selective Nrf2 inhibitor ML385^[11] in IL-13-stimulated BEAS-2B cells. Western blot analysis confirmed that while IL-13 suppressed nuclear Nrf2 translocation and downregulated downstream targets HO-1 and NQO1, FAD treatment effectively restored their expression; however, ML385 co-treatment largely abrogated this effect (Fig. 6A), validating successful Nrf2 pathway inhibition. Functionally, this molecular blockade translated to loss of cytoprotective effects, as demonstrated by CCK-8 assays showing that while FAD rescued IL-13-induced viability suppression, ML385 significantly attenuated this protective response (Fig. 6B). Similarly, flow cytometric analysis revealed that FAD's anti-apoptotic effects against IL-13-induced cell death were substantially compromised by Nrf2 inhibition (Fig. 6C). The Nrf2-dependency extended to antioxidant responses, where

ML385 co-treatment markedly attenuated FAD's ability to restore SOD, CAT, and GSH-Px activities and reduce MDA accumulation in IL-13-challenged cells (Fig. 6D-G). Consistent with these findings, ML385 also partially reversed FAD's suppression of pro-inflammatory cytokines (IL-1 β , IL-18, TNF- α) (Fig. 6H-J). These validation studies suggest that Nrf2 pathway activation is indispensable for FAD's protective mechanisms, establishing this signaling cascade as the critical mediator of FAD's therapeutic efficacy.

Nrf2 Pathway is Essential for FAD's Therapeutic Effects in OVA-Induced Asthmatic Mice

To establish FAD's *in vivo* dependency on Nrf2 signaling, we employed lentiviral-mediated Nrf2 knockdown in OVA-induced asthmatic mice. Western blot analysis confirmed that while FAD effectively restored OVA-suppressed nuclear Nrf2, HO-1, and NQO1 expression, Nrf2 knockdown abolished this molecular restoration (Fig. 7A). This molecular disruption translated to compromised therapeutic efficacy, as histopathological assessment revealed that Nrf2 knockdown significantly diminished FAD's protective effects against airway inflammation, bronchial wall thickening, and smooth muscle hypertrophy (Fig. 7B). The Nrf2-dependency extended across multiple parameters: FAD's suppression of serum IgE elevation was partially reversed in Nrf2-deficient mice (Fig. 7C), while reductions in BALF inflammatory cell infiltration were substantially compromised (Fig. 7D). Similarly, FAD's antioxidant benefits—including restored SOD, CAT, and GSH-Px activities and reduced MDA levels—were markedly attenuated by Nrf2 knockdown (Fig. 7E), as was suppression of pro-inflammatory cytokines in BALF (Fig. 7F). These genetic validation studies demonstrate that Nrf2 activation is

essential for FAD's therapeutic effects in experimental asthma.

Discussion

This study demonstrates that falcarindiol (FAD), a natural polyacetylene compound, exerts therapeutic effects against allergic asthma through Nrf2 pathway-dependent mechanisms. Our findings reveal that FAD treatment significantly ameliorated key features of experimental asthma, including airway inflammation, oxidative stress, immune cell infiltration, and epithelial dysfunction, with therapeutic efficacy comparable to dexamethasone. Critically, both pharmacological inhibition with ML385 and genetic knockdown of Nrf2 suppressed FAD's protective effects, suggesting Nrf2 activation as an essential mediator of FAD's anti-asthmatic properties. These results validate the Nrf2 pathway as a promising target for developing natural product-based therapeutic interventions and suggest that FAD represents a potential mechanism-based approach for asthma management with reduced adverse effects compared to conventional therapies.

In recent years, monomeric components isolated from traditional Chinese medicine (TCM) have attracted significant attention for their therapeutic roles in asthma treatment, owing to their low toxicity and minimal side effects^[21-23]. Falcarindiol, a polyacetylene compound, is present in various edible Apiaceae plants, including celery, celery root, fennel, and parsley, and can also be extracted from carrots and *Notopterygium incisum*^[24]. A growing body of research has demonstrated that falcarindiol exhibits significant antitumor, anti-inflammatory, antifungal, and metabolic regulatory effects through diverse molecular mechanisms^[25-29]. Notably, falcarindiol demonstrates remarkable pathway selectivity, as evidenced by its ability to suppress malignant progression and

induce ferroptosis in non-small cell lung cancer via JAK/STAT3 axis modulation^[28], while simultaneously alleviating neuroinflammation after spinal cord injury through inhibition of STAT/MAPK signaling pathways^[29]. This pathway diversity suggests that falcarindiol can selectively target different signaling cascades depending on the pathological context. Furthermore, studies have indicated that falcarindiol demonstrates stable pharmacological properties and favorable bioavailability *in vivo*^[26]. In our OVA-induced murine asthma model, falcarindiol significantly suppressed oxidative stress levels, alleviated airway inflammation and immune cell infiltration, and ameliorated pulmonary histopathological damage. Furthermore, *in vitro* experiments confirmed its direct inhibitory effects on inflammatory signaling pathways, indicating its capacity to regulate pro-inflammatory cytokine expression. Our findings represent novel evidence linking falcarindiol's anti-inflammatory mechanisms to allergic airway inflammation, laying the foundation for its potential as a therapeutic candidate for asthma.

Asthma pathogenesis is fundamentally characterized by chronic airway inflammation and elevated oxidative stress, which synergistically drive disease progression and severity^[30,31]. Oxidative stress not only correlates with inflammatory biomarkers and airway remodeling indices but also serves as a critical mediator linking environmental exposures to asthmatic manifestations^[30,31]. Given this pathophysiological context, therapeutic interventions targeting both inflammatory cascades and oxidative pathways represent promising strategies for comprehensive asthma management. Falcarindiol has demonstrated robust anti-inflammatory properties across multiple experimental models, effectively preventing inflammation and neoplastic transformation through modulation of key signaling networks^[32,33]. Mechanistic

studies reveal that falcarindiol attenuates inflammation by inhibiting MAPK and JAK-STAT signaling pathways in murine macrophages^[33], while also suppressing dendritic cell maturation, a critical component of adaptive immune responses^[34]. Our *in vivo* findings corroborate these mechanistic insights, demonstrating that falcarindiol treatment significantly reduced inflammatory cell infiltration in lung tissues, including eosinophils and lymphocytes, while simultaneously suppressing pro-inflammatory cytokine production. Furthermore, our data revealed that falcarindiol effectively decreased the production of IgE and tissue damages. These convergent findings demonstrate that falcarindiol possesses broad anti-inflammatory and immunomodulatory capabilities that can effectively address the complex inflammatory milieu characteristic of asthmatic airways.

Beyond its anti-inflammatory properties, falcarindiol demonstrates potent antioxidant capabilities through activation of the Nrf2 signaling pathway, a master regulator of cellular antioxidant defense mechanisms that coordinates the basal and oxidative stress-induced activation of a vast array of cytoprotective genes including antioxidant enzymes, detoxification proteins, and anti-inflammatory mediators^[19,35-38]. Mechanistically, falcarindiol activates the Nrf2/antioxidant response element (ARE) pathway via S-alkylation of cysteine 151 in the Keap1 protein, leading to Nrf2 nuclear translocation and subsequent transcriptional activation of antioxidant genes^[19]. As a transcription factor, Nrf2 induces the expression of numerous cytoprotective enzymes, including heme oxygenase-1 (HO-1), NAD(P)H quinone oxidoreductase, and glutathione S-transferases, which collectively enhance cellular resistance to oxidative damage ^[37,38]. Additionally, falcarindiol functions as a PPAR γ modulator that mediates endoplasmic

reticulum stress-mediated responses by regulating NOX4, further contributing to its antioxidant effects^[35]. Notably, falcarindiol has been shown to be more effective than sulforaphane, a well-established Nrf2 activator, in attenuating intestinal inflammation at diet-achievable doses^[36]. The therapeutic potential of antioxidant-based interventions in asthma has been supported by studies demonstrating that natural compounds with antioxidant properties, such as R8 (a semi-synthetic vasicine analogue) and safranal from *Crocus sativus*, attenuate allergic airway inflammation through reduced oxidative stress^[39,40]. Our experimental findings align with these mechanistic insights, demonstrating that falcarindiol treatment significantly upregulated antioxidant enzyme activities, including superoxide dismutase, catalase, and glutathione peroxidase, in lung tissues of OVA-challenged mice. Furthermore, our data revealed enhanced Nrf2 nuclear translocation and increased expression of downstream antioxidant genes following falcarindiol administration. These results suggest that falcarindiol's therapeutic efficacy in asthma may stem from its dual capacity to suppress inflammatory pathways while simultaneously fortifying cellular antioxidant defenses.

In summary, this study systematically elucidates the dual anti-inflammatory and antioxidant mechanisms of falcarindiol in allergic asthma through integrated *in vivo* and *in vitro* approaches. Our findings demonstrate that falcarindiol significantly alleviates airway inflammation, suppresses immune cell infiltration, and mitigates oxidative stress via activation of the Nrf2 signaling pathway (Figure 8). This mechanistic insight reveals a novel therapeutic pathway whereby falcarindiol simultaneously targets inflammatory cascades and oxidative stress responses, providing both theoretical

foundation and experimental validation for its potential as a naturally derived, low-toxicity therapeutic candidate. Future investigations should evaluate its long-term efficacy and safety profiles in chronic airway diseases to advance innovative asthma intervention strategies.

Abbreviations

ANOVA - Analysis of variance

ARE - Antioxidant response element

BALF - Bronchoalveolar lavage fluid

BCA - Bicinchoninic acid

BSA - Bovine serum albumin

CAT - Catalase

CCK-8 - Cell Counting Kit-8

DAPI - 4',6-diamidino-2-phenylindole

DEX - Dexamethasone

ECL - Enhanced chemiluminescence

EdU - 5-ethynyl-2'-deoxyuridine

ELISA - Enzyme-linked immunosorbent assay

FAD - Falcarindiol

FBS - Fetal bovine serum

FITC - Fluorescein isothiocyanate

GSH-Px - Glutathione peroxidase

H&E - Hematoxylin and eosin

HO-1 - Heme oxygenase-1

HRP - Horseradish peroxidase

HSD - Honest significant difference

IgE - Immunoglobulin E

IL - Interleukin

Keap1 - Kelch-like ECH-associated protein 1

MDA - Malondialdehyde
NQO1 - NAD(P)H quinone dehydrogenase 1
Nrf2/NRF2 - Nuclear factor erythroid 2-related factor 2
OVA - Ovalbumin
Pbm - Perimeter of basement membrane
PBS - Phosphate-buffered saline
PI - Propidium iodide
PVDF - Polyvinylidene fluoride
RIPA - Radioimmunoprecipitation assay
SD - Standard deviation
SDS-PAGE - Sodium dodecyl sulfate-polyacrylamide gel electrophoresis
shRNA - Short hairpin RNA
SOD - Superoxide dismutase
TCM - Traditional Chinese medicine
TdT - Terminal deoxynucleotidyl transferase
TNF- α - Tumor necrosis factor alpha
TUNEL - Terminal deoxynucleotidyl transferase dUTP nick end labeling
Wall/Pbm - Airway wall thickness to perimeter ratio
Wasm/Pbm - Airway smooth muscle thickness to perimeter ratio
WHO - World Health Organization

DECLARATIONS

Ethics approval and consent to participate

This study was reviewed and approved by the Ethics Committee of Longyan First Hospital. Each experiment was performed in accordance with the National Institute of Health Guide for the Care and Use of Laboratory Animals. The study was carried out in

compliance with the ARRIVE guidelines (<https://arriveguidelines.org>).

Consent for publication

Not applicable

Availability of data and material

The datasets generated and/or analyzed during the current study are available from the corresponding author upon reasonable request.

Disclosure of conflict of interest

The authors declared that there was no conflict of interest associated with the manuscript.

Funding

Not applicable.

Authors' contributions

XH Jiang, SX Lai and HF Wu contributed to literature review, study design, manuscript writing and critical reversion, and preparation of Figure 1-7. Z Lin, and FH Lai were in charge of data extraction, analysis and interpretation. All authors read and agreed to this eventual version for publication.

Acknowledgements

Not applicable.

References

- [1] Gans MD, Gavrilova T: Understanding the immunology of asthma: Pathophysiology, biomarkers, and treatments for asthma endotypes. *Paediatr Respir Rev* 2020, 36:118-27.
- [2] Miller RL, Grayson MH, Strothman K: Advances in asthma: New understandings of asthma's natural history, risk factors, underlying mechanisms, and clinical management. *J Allergy Clin Immunol* 2021, 148(6):1430-41.
- [3] Cazzola M, Rogliani P, Ora J, et al.: Asthma and comorbidities:

- recent advances. *Pol Arch Intern Med* 2022, 132(4).
- [4] Bosi A, Tonelli R, Castaniere I, et al.: Acute severe asthma: management and treatment. *Minerva Med* 2021, 112(5):605-14.
- [5] Papadopoulos NG, Miligkos M, Xepapadaki P: A Current Perspective of Allergic Asthma: From Mechanisms to Management. *Handb Exp Pharmacol* 2022, 268(69-93).
- [6] Komlosi ZI, van de Veen W, Kovacs N, et al.: Cellular and molecular mechanisms of allergic asthma. *Mol Aspects Med* 2022, 85:100995.
- [7] Holgate ST, Wenzel S, Postma DS, et al.: Asthma. *Nat Rev Dis Primers* 2015, 1(1):15025.
- [8] Scadding GK, Scadding GW: Innate and adaptive immunity in allergic airway disease. *Curr Opin Allergy Clin Immunol* 2022, 22(1):10-5.
- [9] Noel JC, Berin MC: Role of innate immunity and myeloid cells in susceptibility to allergic disease. *Ann N Y Acad Sci* 2021, 1499(1):42-53.
- [10] Minnicozzi M, Sawyer RT, Fenton MJ: Innate immunity in allergic disease. *Immunol Rev* 2011, 242(1):106-27.
- [11] Audousset C, McGovern T, Martin JG: Role of Nrf2 in Disease: Novel Molecular Mechanisms and Therapeutic Approaches - Pulmonary Disease/Asthma. *Front Physiol* 2021, 12:727806.
- [12] Li L, Chen Y, Jiao D, et al.: Protective Effect of Astaxanthin on Ochratoxin A-Induced Kidney Injury to Mice by Regulating Oxidative Stress-Related NRF2/KEAP1 Pathway. *Molecules* 2020, 25(6).
- [13] Xu C, Song Y, Wang Z, et al.: Pterostilbene suppresses oxidative stress and allergic airway inflammation through AMPK/Sirt1 and Nrf2/HO-1 pathways. *Immun Inflamm Dis* 2021, 9(4):1406-17.
- [14] Wang Y, Zhang M, Bi R, et al.: ACSL4 deficiency confers

protection against ferroptosis-mediated acute kidney injury. *Redox Biol* 2022, 51(102262).

[15] Park KR, Leem HH, Kwon YJ, et al.: Falcarindiol Stimulates Apoptotic and Autophagic Cell Death to Attenuate Cell Proliferation, Cell Division, and Metastasis through the PI3K/AKT/mTOR/p70S6K Pathway in Human Oral Squamous Cell Carcinomas. *Am J Chin Med.* 2022;50(1):295-311.

[16] Wyrembek P, Negri R, Kaczor P, et al.: Falcarindiol allosterically modulates GABAergic currents in cultured rat hippocampal neurons. *J Nat Prod.* 2012 Apr 27;75(4):610-6.

[17] Ghanadian M, Sadraei H, Asghari G, et al.: Bioassay-directed isolation of falcarindiol and isoacetovanillon from *Pycnocyclus caespitosus* based on KCl-induced contraction in rat uterus smooth muscles. *Res Pharm Sci* 2017, 12(3):249-56.

[18] Deding U, Clausen BH, Al-Najami I, et al.: Effect of Oral Intake of Carrot Juice on Cyclooxygenases and Cytokines in Healthy Human Blood Stimulated by Lipopolysaccharide. *Nutrients.* 2023 Jan 26;15(3):632.

[19] Ohnuma T, Nakayama S, Anan E, et al.: Activation of the Nrf2/ARE pathway via S-alkylation of cysteine 151 in the chemopreventive agent-sensor Keap1 protein by falcarindiol, a conjugated diacetylene compound. *Toxicol Appl Pharmacol* 2010, 244(1):27-36.

[20] Ohnuma T, Anan E, Hoashi R, et al.: Dietary diacetylene falcarindiol induces phase 2 drug-metabolizing enzymes and blocks carbon tetrachloride-induced hepatotoxicity in mice through suppression of lipid peroxidation. *Biol Pharm Bull.* 2011;34(3):371-8.

[21] Meng Z, Chen H, Deng C, et al.: Potential cellular endocrinology mechanisms underlying the effects of Chinese herbal

medicine therapy on asthma. *Front Endocrinol (Lausanne)* 2022, 13(916328).

[22] Wang W, Yao Q, Teng F, et al.: Active ingredients from Chinese medicine plants as therapeutic strategies for asthma: Overview and challenges. *Biomed Pharmacother* 2021, 137(111383).

[23] Yuan JY, Tong ZY, Dong YC, et al.: Research progress on icariin, a traditional Chinese medicine extract, in the treatment of asthma. *Allergol Immunopathol (Madr)* 2022, 50(1):9-16.

[24] Andersen CB, Runge Walther A, Pipo-Olle E, et al.: Falcarindiol Purified From Carrots Leads to Elevated Levels of Lipid Droplets and Upregulation of Peroxisome Proliferator-Activated Receptor-gamma Gene Expression in Cellular Models. *Front Pharmacol* 2020, 11(565524).

[25] Kan S, Tan J, Cai Q, et al.: Synergistic activity of the combination of falcarindiol and itraconazole in vitro against dermatophytes. *Front Cell Infect Microbiol* 2023, 13(1128000).

[26] Kobaek-Larsen M, Nielsen DS, Kot W, et al.: Effect of the dietary polyacetylenes falcarinol and falcarindiol on the gut microbiota composition in a rat model of colorectal cancer. *BMC Res Notes* 2018, 11(1):411.

[27] Takahashi S, Okaze H, Kawamoto S: Falcarindiol promotes beige adipocyte-related gene expression and mitochondrial respiration in human preadipocyte-derived adipocytes. *Cytotechnology* 2025, 77(4):125.

[28] Shi Z, Shen Y, Liu X, et al.: Falcarindiol Suppresses Malignant Progression and Induces Ferroptosis in Non-Small Cell Lung Cancer by Regulating JAK/STAT3 Axis. *J Biochem Mol Toxicol* 2025, 39(9):e70486.

[29] Cao L, Huang X, Zhu J, et al.: Falcarindiol improves functional recovery and alleviates neuroinflammation after spinal cord injury

by inhibiting STAT/MAPK signaling pathways. *Biochem Biophys Res Commun* 2024, 736:150860.

[30] Bazan-Socha S, Wójcik K, Olchawa M, et al.: Increased Oxidative Stress in Asthma-Relation to Inflammatory Blood and Lung Biomarkers and Airway Remodeling Indices. *Biomedicines*. 2022 Jun 24;10(7):1499.

[31] Shen G, Yang Y, Wang N, et al.: Association of life's essential 8 and asthma: mediating effect of inflammation and oxidative stress. *J Asthma*. 2025 Feb;62(2):328-335.

[33] Alfurayhi R, Huang L, Brandt K. Pathways Affected by Falcarinol-Type Polyacetylenes and Implications for Their Anti-Inflammatory Function and Potential in Cancer Chemoprevention. *Foods*. 2023 Mar 11;12(6):1192.

[32] Kobaek-Larsen M, Baatrup G, KhataeiNotabi M, et al.: Dietary Polyacetylenic Oxylipins Falcarinol and Falcarindiol Prevent Inflammation and Colorectal Neoplastic Transformation: A Mechanistic and Dose-Response Study in A Rat Model. *Nutrients* 2019, 11(9).

[33] Venkatesan T, Choi YW, Lee J, et al.: Falcarindiol inhibits LPS-induced inflammation via attenuating MAPK and JAK-STAT signaling pathways in murine macrophage RAW 264.7 cells. *Mol Cell Biochem*. 2018 Aug;445(1-2):169-178.

[34] Mitsui S, Torii K, Fukui H, et al.: The herbal medicine compound falcarindiol from *Notopterygii Rhizoma* suppresses dendritic cell maturation. *J Pharmacol Exp Ther*. 2010 Jun;333(3):954-60.

[35] Kim TW, Ko SG. A Novel PPAR γ Modulator Falcarindiol Mediates ER Stress-Mediated Apoptosis by Regulating NOX4 and Overcomes Radioresistance in Breast Cancer. *Antioxidants (Basel)*. 2024 Dec 14;13(12):1533.

[36] Stefanson AL, Bakovic M. Falcarinol Is a Potent Inducer of

Heme Oxygenase-1 and Was More Effective than Sulforaphane in Attenuating Intestinal Inflammation at Diet-Achievable Doses. *Oxid Med Cell Longev*. 2018 Oct 21;2018:3153527.

[37] Arisawa K, Natori M, Hiranuma T, et al.: NRF2-dependent suppression of selenoprotein P expression promotes intracellular selenium metabolic remodeling and upregulation of antioxidant selenoproteins in hepatocellular carcinoma. *Redox Biol*. 2025 Aug 13;86:103821.

[38] Ngo V, Duennwald ML. Nrf2 and Oxidative Stress: A General Overview of Mechanisms and Implications in Human Disease. *Antioxidants (Basel)*. 2022 Nov 27;11(12):2345.

[39] Rayees S, Mabalirajan U, Bhat WW, et al.: Therapeutic effects of R8, a semi-synthetic analogue of Vasicine, on murine model of allergic airway inflammation via STAT6 inhibition. *Int Immunopharmacol*. 2015 May;26(1):246-56. \

[40] Bukhari SI, Pattnaik B, Rayees S, et al.: Safranal of *Crocus sativus* L. inhibits inducible nitric oxide synthase and attenuates asthma in a mouse model of asthma. *Phytother Res*. 2015 Apr;29(4):617-27.

Figure legends

Figure 1. FAD Dose-Dependently Ameliorates Airway Inflammation and Immune Responses in OVA-Induced Asthmatic Mice

Mice were divided into five groups (n=6 per group): Sham control, OVA-induced asthma model, OVA + FAD (100 mg/kg), OVA + FAD (200 mg/kg), and OVA + dexamethasone (DEX, 1 mg/kg) positive control. (A) Hematoxylin-eosin (H&E) staining of lung tissue sections showing histopathological changes, with quantitative analysis of

inflammation scores, airway wall thickness (Wall/Pbm), and airway smooth muscle thickness (Wasm/Pbm). (B) PAS staining of mucus-secreting goblet cells in lung tissues. (C) Enzyme-linked immunosorbent assay (ELISA) analysis of total IgE, ovalbumin-specific IgE, IL-4 and IL-5 levels in serum samples. (D) Immune cell infiltration analysis in bronchoalveolar lavage fluid (BALF) using a hematology analyzer: quantification of total leukocyte counts, absolute eosinophil counts, and eosinophil percentages. (E) Semi-quantitative respiratory distress scores following methacholine challenge. Mice were nebulized with methacholine (25 mg/mL) for 30 seconds and respiratory patterns were observed for 5 minutes. Distress was scored on a 0-4 scale by blinded observers. *, $P < 0.05$; **, $P < 0.01$; ***, $P < 0.001$.

Figure 2. FAD Attenuates Oxidative Stress and Inflammatory Responses Concurrent with Nrf2 Pathway Activation in Asthmatic Mice

Experimental groups were identical to Figure 1 (n=6 per group). (A-D) Biochemical analysis of oxidative stress markers in lung tissue homogenates: malondialdehyde (MDA) levels and activities of superoxide dismutase (SOD), catalase (CAT), and glutathione peroxidase (GSH-Px). (E-G) ELISA quantification of pro-inflammatory cytokines IL-1 β , IL-18, and TNF- α in BALF samples. (H-J) ELISA measurement of systemic inflammatory cytokines IL-1 β , IL-18, and TNF- α in serum samples. (K) Western blot analysis of nuclear Nrf2 translocation and downstream target proteins HO-1 and NQO1 expression in lung tissues. *, $P < 0.05$; **, $P < 0.01$; ***, $P < 0.001$.

Figure 3. FAD Suppresses Apoptosis and Restores

Proliferation in Pulmonary Epithelial Cells of Asthmatic Mice

Experimental groups were identical to Figure 1 (n=6 per group). (A) Terminal deoxynucleotidyl transferase dUTP nick end labeling (TUNEL) staining of lung tissue sections to detect apoptotic cells (red fluorescence) with DAPI nuclear counterstaining (blue), including quantitative analysis of TUNEL-positive cell counts. (B) Ki67 immunofluorescence staining of lung tissue sections to assess cellular proliferation (red fluorescence) with DAPI counterstaining (blue), including quantitative analysis of Ki67-positive cell numbers. *, P < 0.05; **, P < 0.01; ***, P < 0.001.

Figure 4. FAD Protects BEAS-2B Cells Against IL-13-Induced Cytotoxicity and Proliferation Suppression

Bronchial epithelial BEAS-2B cells were divided into groups: untreated control, IL-13 stimulation (10 ng/mL), and IL-13 + FAD treatment (5, 10, 20 μ M). (A) Cell Counting Kit-8 (CCK-8) viability assay to evaluate FAD cytotoxicity across concentrations (0-50 μ M). (B) CCK-8 analysis assessing FAD's protective effects against IL-13-induced cell viability suppression. (C) 5-ethynyl-2'-deoxyuridine (EdU) incorporation assay with immunofluorescence detection (red) and DAPI nuclear counterstaining (blue), including quantification of EdU-positive proliferating cells. (D) Flow cytometric analysis of apoptosis using Annexin V-FITC/propidium iodide double staining. N=3 independent experiments. *, P < 0.05; **, P < 0.01; ***, P < 0.001.

Figure 5. FAD Alleviates IL-13-Induced Oxidative Stress and Inflammation Concurrent with Nrf2 Pathway Activation in BEAS-2B Cells

Experimental groups were identical to Figure 4 (N=3 independent

experiments). (A-D) Biochemical analysis of cellular oxidative stress: activities of SOD, CAT, and GSH-Px enzymes, and MDA levels in cell lysates. (E-G) ELISA quantification of pro-inflammatory cytokines IL-1 β , IL-18, and TNF- α in cell culture supernatants. (H) Western blot analysis of nuclear Nrf2 translocation and downstream antioxidant proteins HO-1 and NQO1 expression in cell lysates. *, P < 0.05; **, P < 0.01; ***, P < 0.001.

Figure 6. Nrf2 Pathway Inhibition Abrogates FAD's Protective Effects in IL-13-Stimulated BEAS-2B Cells

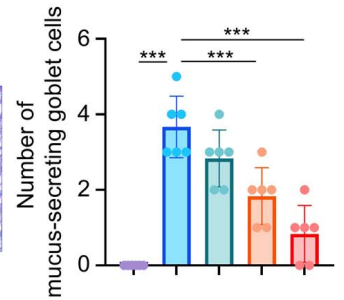
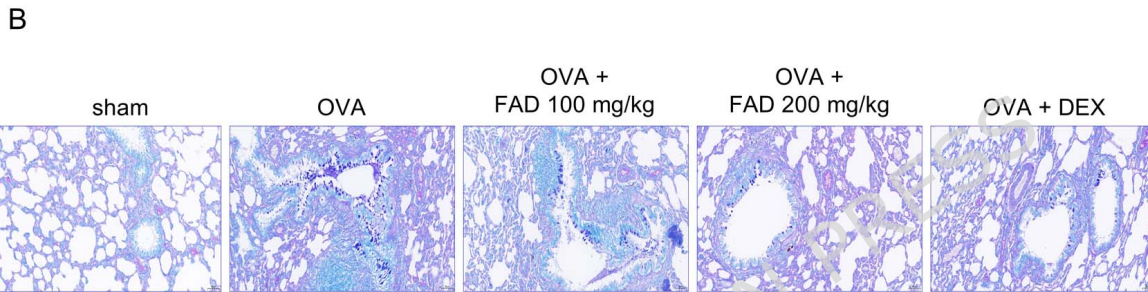
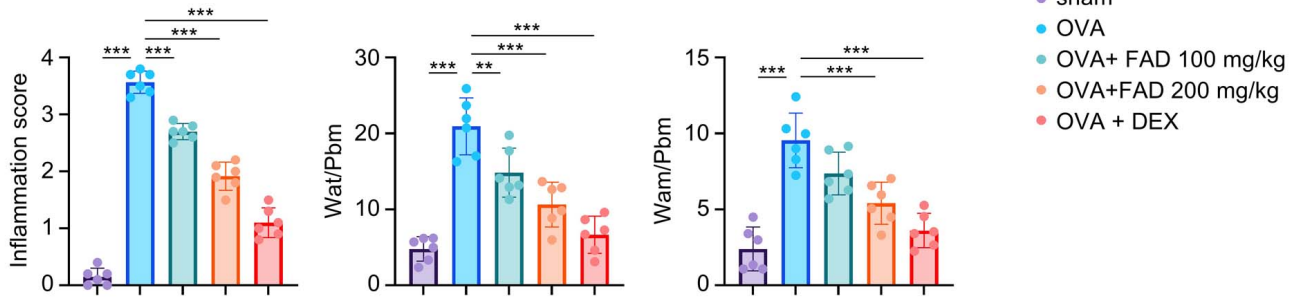
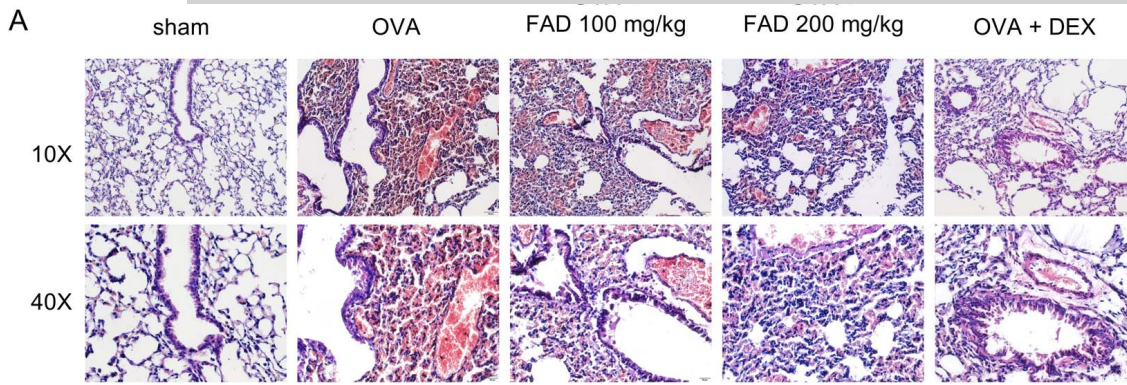
BEAS-2B cells were divided into four groups: untreated control, IL-13 stimulation (10 ng/mL), IL-13 + FAD (20 μ M), and IL-13 + FAD + ML385 (Nrf2 inhibitor, 10 μ M). (A) Western blot analysis of nuclear Nrf2, HO-1, and NQO1 protein expression to validate Nrf2 pathway inhibition. (B) CCK-8 viability assay evaluating the impact of Nrf2 inhibition on FAD's cytoprotective effects. (C) Flow cytometric apoptosis analysis using Annexin V-FITC/propidium iodide staining. (D-G) Biochemical assessment of oxidative stress markers: SOD, CAT, and GSH-Px enzyme activities, and MDA levels. (H-J) ELISA quantification of inflammatory cytokines IL-1 β , IL-18, and TNF- α in culture supernatants. N=3 independent experiments. *, P < 0.05; **, P < 0.01; ***, P < 0.001.

Figure 7. Genetic Nrf2 Knockdown Abolishes FAD's Therapeutic Effects in OVA-Induced Asthmatic Mice

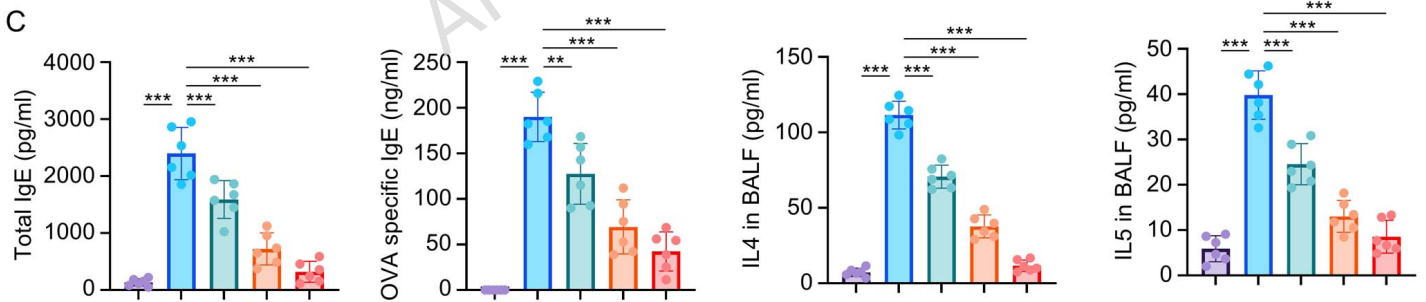
Mice were divided into four groups (n=6 per group): Sham + lentiviral negative control shRNA, OVA + lentiviral negative control shRNA, OVA + FAD (200 mg/kg) + lentiviral negative control shRNA, and OVA + FAD (200 mg/kg) + lentiviral Nrf2-targeting shRNA. (A) Western blot analysis of nuclear Nrf2, HO-1, and NQO1 protein

expression in lung tissues to confirm Nrf2 knockdown efficiency. (B) H&E staining of lung tissue sections with morphometric analysis of inflammation scores, airway wall thickness (Wall/Pbm), and smooth muscle thickness (Wasm/Pbm). (C) ELISA analysis of total IgE and ovalbumin-specific IgE levels in serum samples. (D) Flow cytometric quantification of BALF inflammatory cells: total CD45⁺ leukocyte counts, absolute eosinophil numbers, and eosinophil percentages. (E) Biochemical analysis of lung tissue oxidative stress markers: SOD, CAT, and GSH-Px activities, and MDA levels. (F) ELISA measurement of pro-inflammatory cytokines IL-1 β , IL-18, and TNF- α in BALF samples. *, P < 0.05; **, P < 0.01; ***, P < 0.001.

Figure 8. Schematic Illustration of the Mechanism by Which Falcarindiol Alleviates Airway Inflammation and Oxidative Stress via Activation of the Nrf2 Pathway

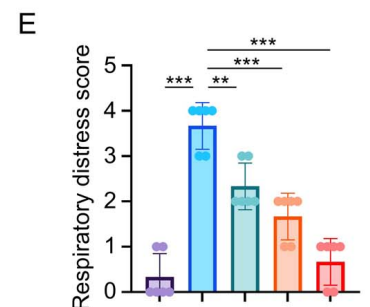
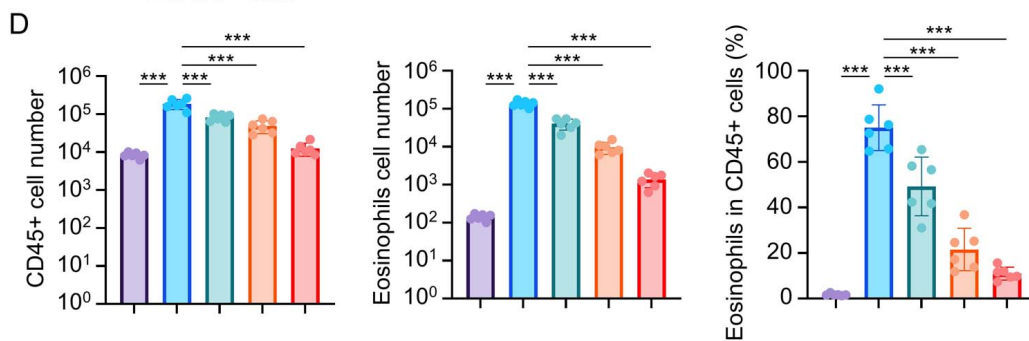


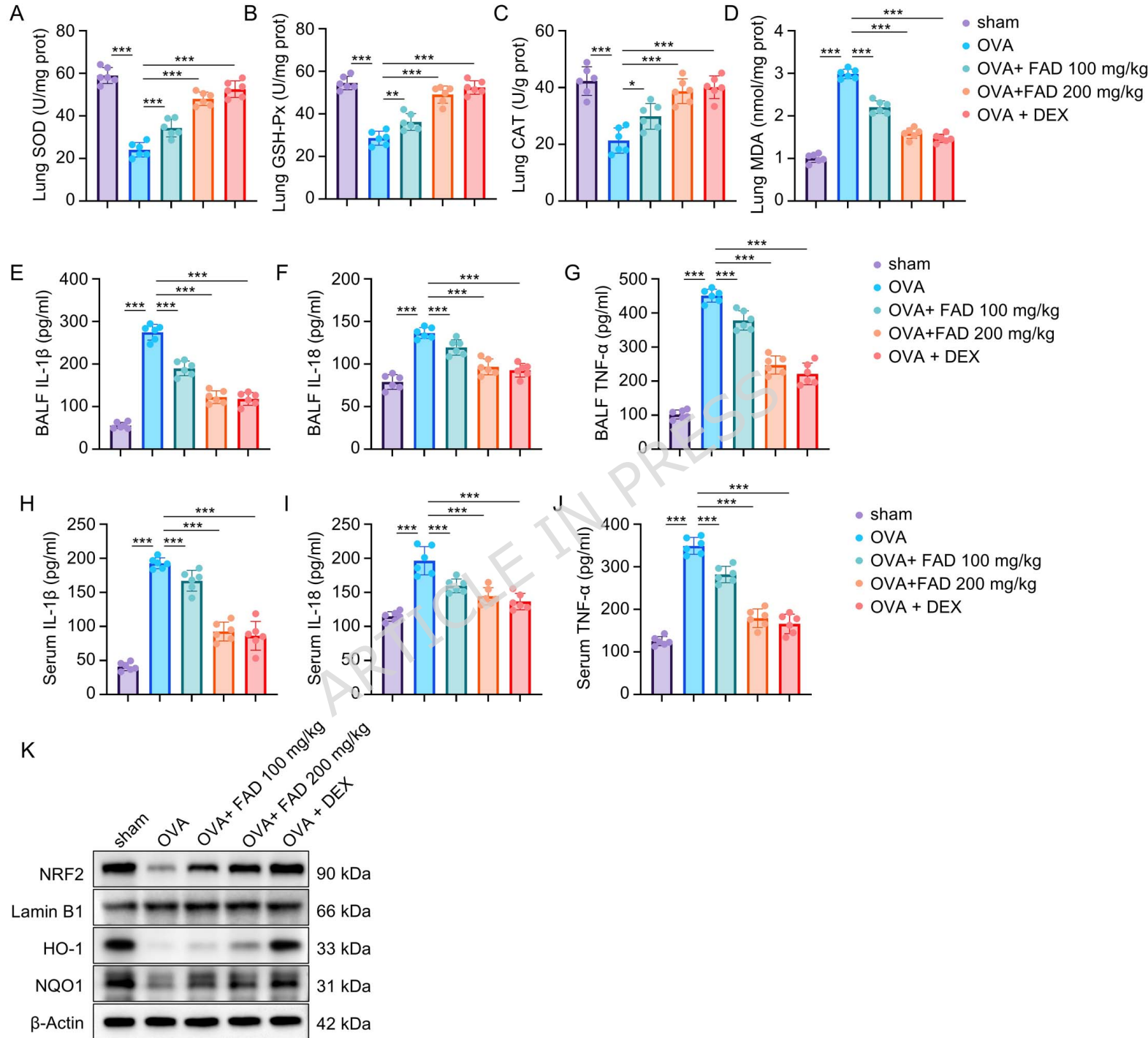
- sham
- OVA
- OVA+ FAD 100 mg/kg
- OVA+FAD 200 mg/kg
- OVA + DEX

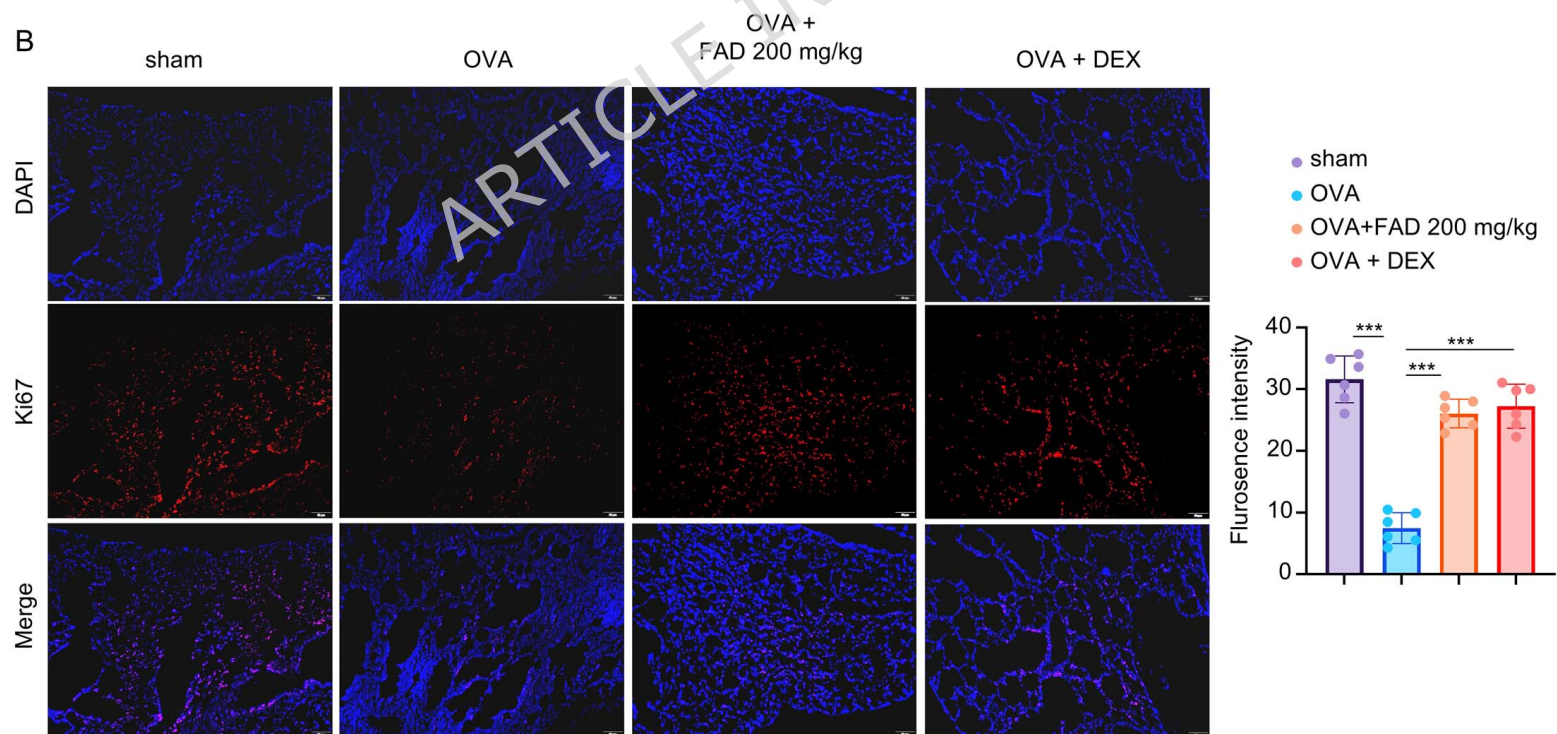
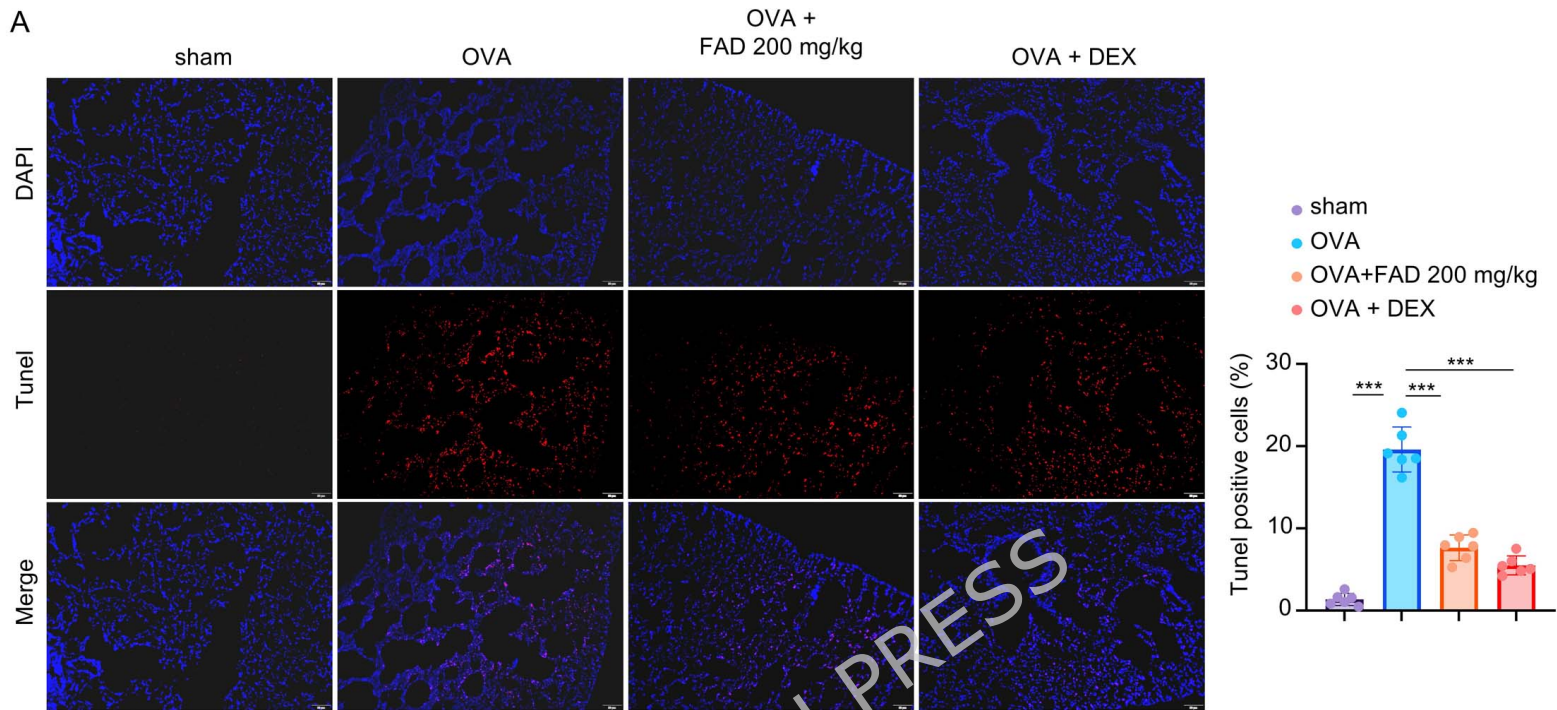


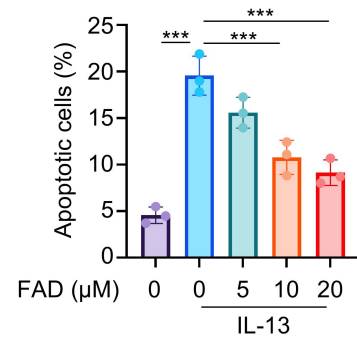
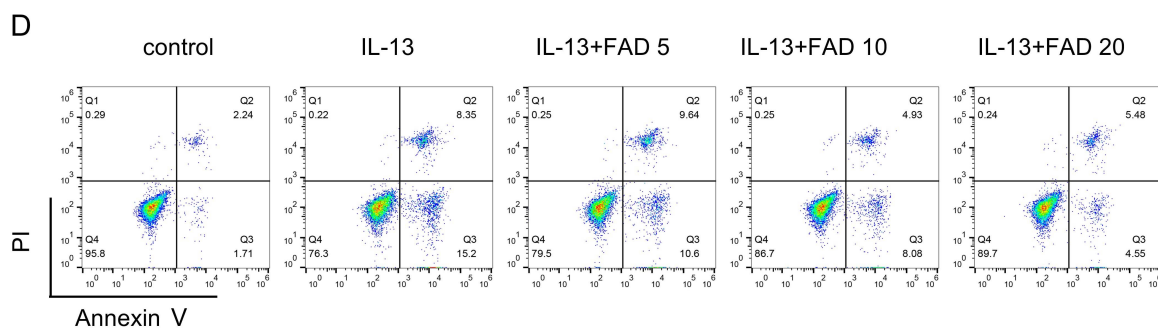
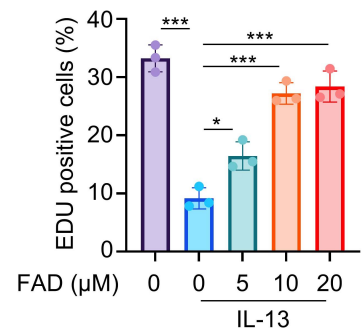
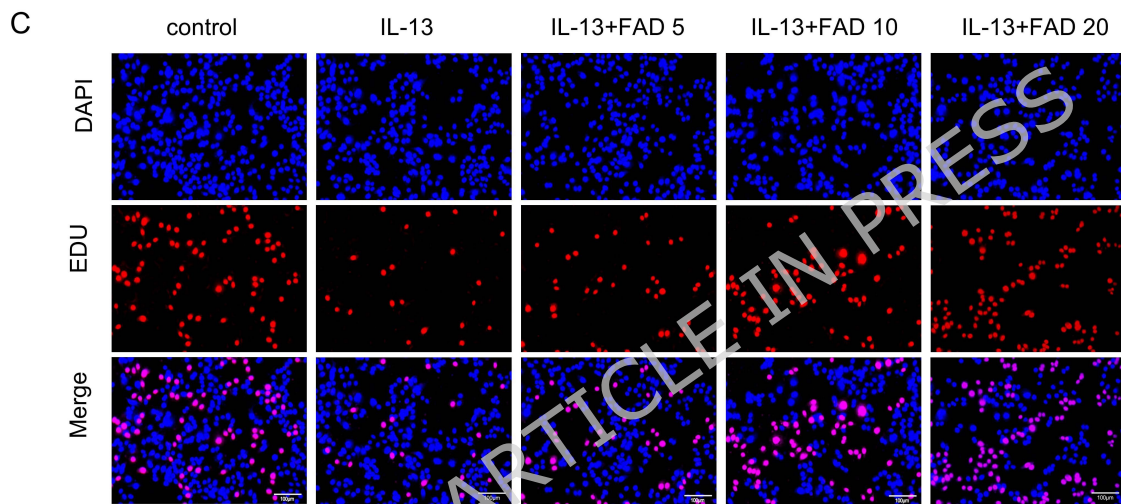
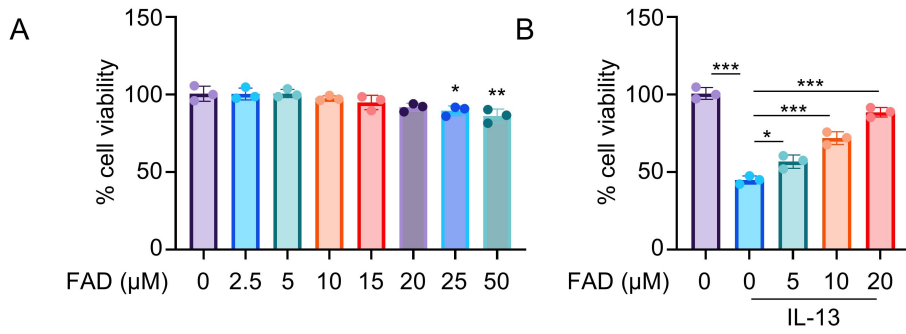
- sham
- OVA
- OVA+ FAD 100 mg/kg
- OVA+FAD 200 mg/kg
- OVA + DEX

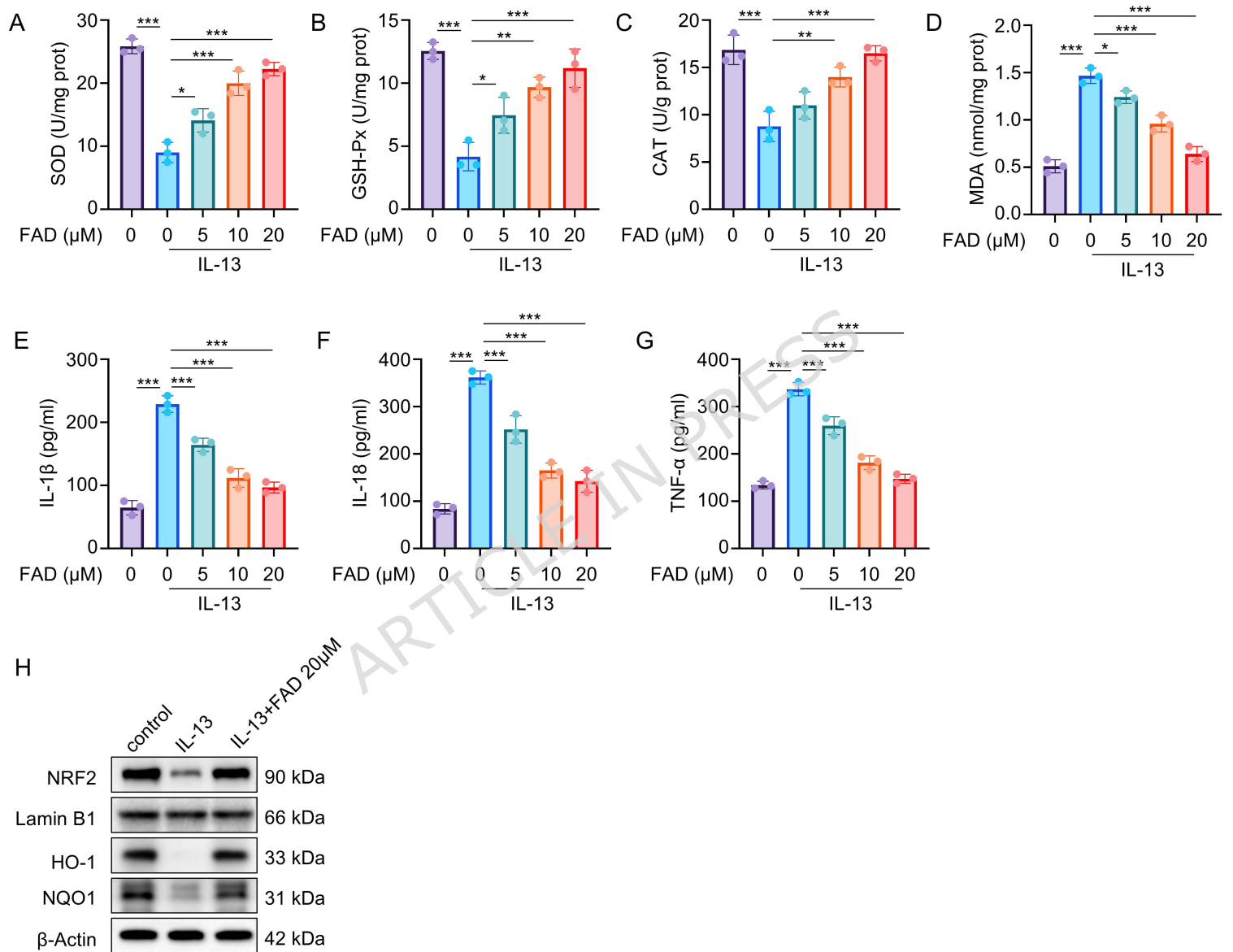
- sham
- OVA
- OVA+ FAD 100 mg/kg
- OVA+FAD 200 mg/kg
- OVA + DEX

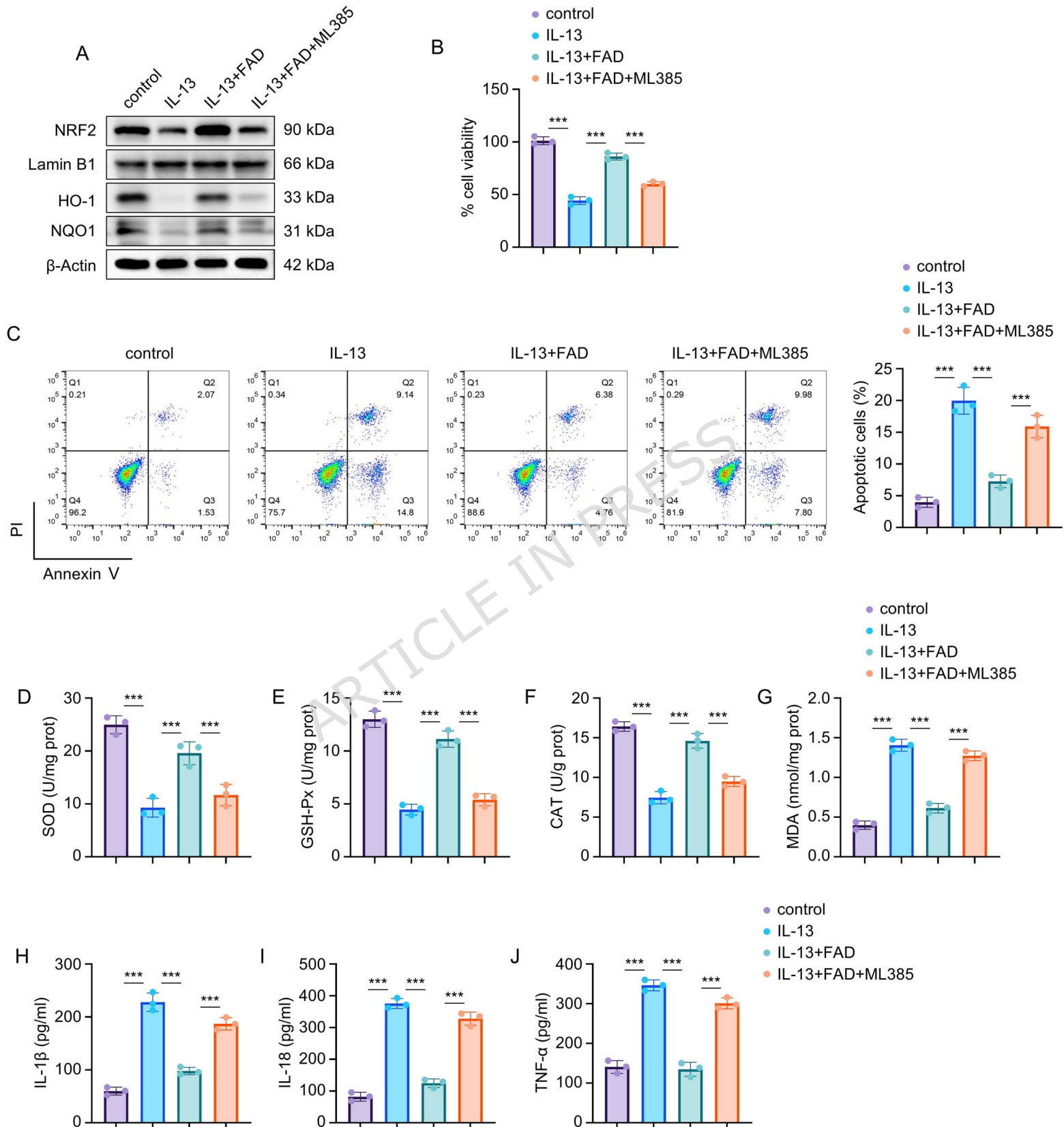


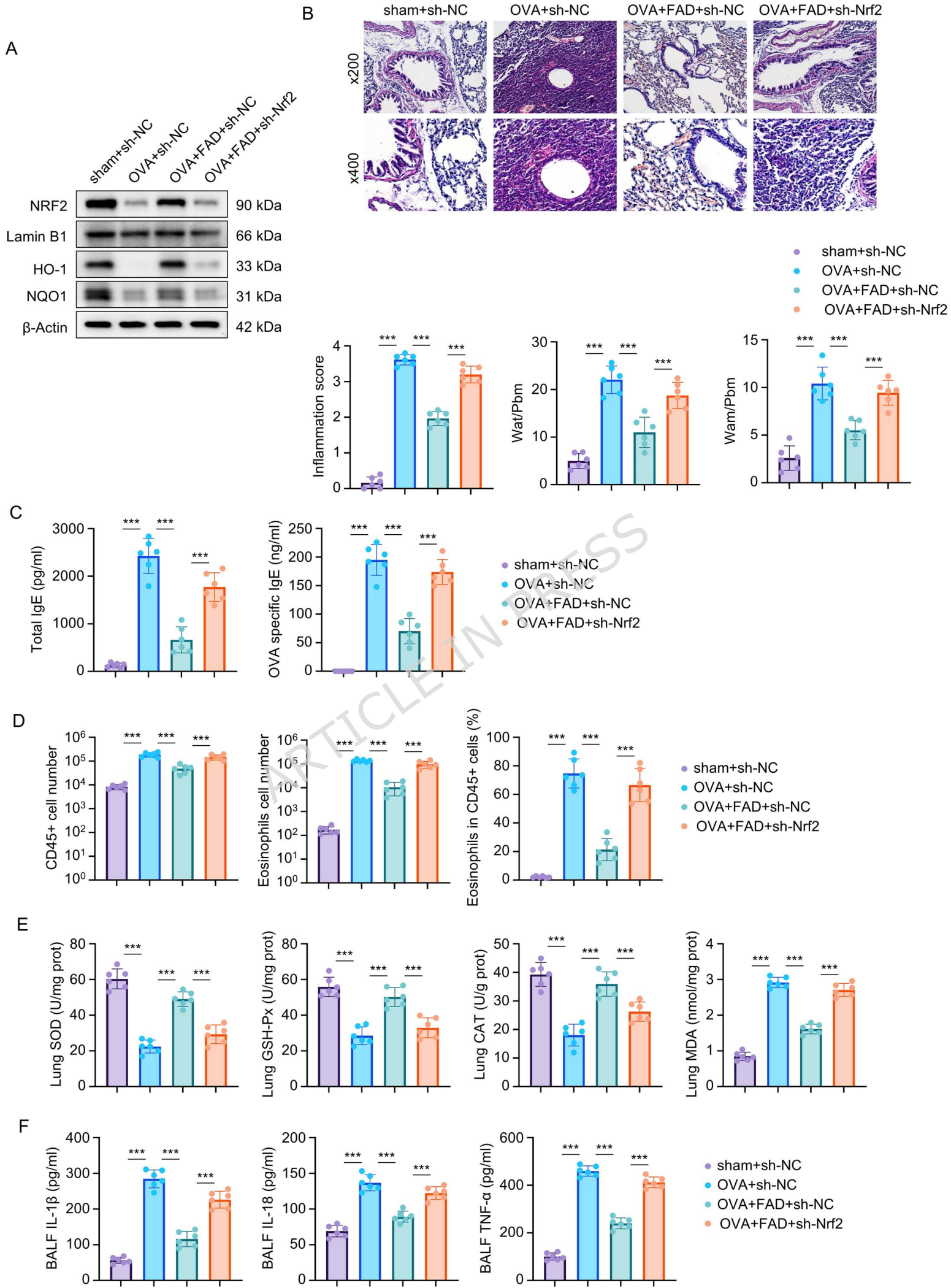












ASTHMATIC AIRWAY (UNTREATED)

FAD-TREATED AIRWAY

